


Article

Parabolic Air Collectors with an Evacuated Tube Containing Copper Tube and Spiral Strip, and a New Cavity Receiver: Experimental Performance Analysis

Ayad K. Khelif¹, Wisam Abed Kattea Al-Maliki^{2,3} , Hasanain A. Abdul Wahhab⁴ , Falah Alobaid^{3,*} , Bernd Epple³ and Akeel A. Abtan¹ 

¹ Department of Electromechanical Engineering, University of Technology-Iraq, Ministry of Higher Education & Scientific Research, Baghdad 10066, Iraq

² Mechanical Engineering Department, University of Technology-Iraq, Baghdad 10066, Iraq

³ TU Darmstadt, Institut Energiesysteme und Energietechnik, Otto-Berndt-Straße 2, 64287 Darmstadt, Germany

⁴ Training and Workshop Center, University of Technology-Iraq, Baghdad 10066, Iraq

* Correspondence: falah.alobaid@est.tu-darmstadt.de

Abstract: Sunray thermal energy is one of the most promising and quickly growing techniques globally. In parabolic trough air collectors (PTAC), receiver design and safety are of paramount importance because of their impact on the overall effectiveness of power plants. However, experimental studies of alternative receivers to improve heat transfer are still to be performed. In this study, a PTAC system was tested experimentally with an evacuated tube: open on one end, containing a copper tube and a spiral strip (case 1), and with a new cavity receiver consisting of several arranged tetragonal pyramidal elements (case 2). Afterward, the results were compared and showed a slightly superior exit air temperature and thermal efficiency performance for case 1. The overall results demonstrate a remarkable convergence of case 2 from case 1 in terms of temperature increase across PTAC, in which the maximum exit air temperature for case 1 is 58.2 °C, a 3.4% increase over case 2 at 0.0105 kg/s mass flow rate. Lastly, the results validate the potential and clarify the specific conclusions of these methods' application in improving heat exchange in a PTAC.

Keywords: sunray air heater; cavity receiver and several arranged quadrangular pyramidal elements; thermal efficiency; parabolic trough collector



Citation: Khelif, A.K.; Al-Maliki, W.A.K.; Abdul Wahhab, H.A.; Alobaid, F.; Epple, B.; Abtan, A.A. Parabolic Air Collectors with an Evacuated Tube Containing Copper Tube and Spiral Strip, and a New Cavity Receiver: Experimental Performance Analysis. *Sustainability* **2023**, *15*, 7926. <https://doi.org/10.3390/su15107926>

Academic Editor: Sergio Nardini

Received: 14 February 2023

Revised: 2 May 2023

Accepted: 3 May 2023

Published: 12 May 2023



Copyright: © 2023 by the authors. Licensee MDPI, Basel, Switzerland. This article is an open access article distributed under the terms and conditions of the Creative Commons Attribution (CC BY) license (<https://creativecommons.org/licenses/by/4.0/>).

1. Introduction

Solar energy is an abundant, environment-friendly, and hygienic energy source, so it is employed to meet the enormous demands of the power and energy sectors [1–3]. The easiest and most effective approach to satisfy such demands is to use sunray energy as a heating source. Sunray air heating systems are used in the food, agricultural, textile, drying, and building heating sectors [4]. Different types of collectors have been utilized for air heating, including evacuated tubes, flat plate collectors for low and medium-temperature air heating, and parabolic trough collectors (PTC) for high-temperature air heating [5–9]. Researchers have recently used various materials to design, develop, and assess parabolic sunray air heaters [10]. Absorbent tube design is one aspect that significantly affects the amount of energy that can be obtained from sunlight [11–13]. Several studies have lately been undertaken on the effect of heat exchanger geometry on sunray collector performance [14–22]. Zou et al. [23] used a U-shaped aluminium tube with black fins to demonstrate a sunray receiver for a small-scale PTC to heat water in low-temperature regions. Receiver absorption is substantially increased by the synthetic black fin tube. The results showed an improvement in thermal efficiency. Fuqiang et al. [24] created an outwardly asymmetric convex corrugated tube to improve an absorber tube's reliability and heat transfer coefficient. The heat transfer performance was improved by 148%, and

the thermal strain was reduced. Zhang et al. explored an experimental double-glazing vacuum U-type PTC receiver that transfers heat via water to increase thermal efficiency [25]. Zinian et al. [15] demonstrated that a flat tube absorber receives 15.9% less energy per year than an evacuated tube collector that has an absorber of semi-cylindrical shape. Okonkwo et al. [16,17] investigated how PTC performed with absorber shape and working fluids, including specific nanofluids. Examples of absorber tube configurations, plain tubes, porous inserts, longitudinally finned tubes, converging-diverging tubes, and tubes with twisted tape inserts were considered. The researchers found that both modifying the absorber tube shape and applying nanofluids significantly improved the thermal performance of the PTC. Demagh et al. [18] presented a study on the viability of using an S-curved/sinusoidal absorber in PTCs. The S-curved absorber received significant sunray energy, and they concluded that it outperformed the conventional straight absorber. Vishwakarma et al. [19] investigated the ability of several helically grooved absorber tube forms, such as rectangular, trapezoidal, triangular, and semicircular forms, to increase the thermal efficiency of parabolic trough sunray collectors (PTSC). The findings indicated that the triangular groove-based absorber tube's thermal performance remained superior. A heat exchanger with fins was proposed to work in the absorber tube more effectively than one without fins [26–29]. Bellos et al. [27] analyzed the location of the fins and their number in PTCs. The bottom section of the absorber was discovered to be the ideal fin location to generate superior outcomes; the presence of more fins led to enhanced performance. The researchers explained that thermal efficiency increased by 0.51% by adding three metal fins in the absorber tube's lower half. Muñoz and Abánades [28] considered tubes' internal fins to determine how they affect the durability of PTCs. They claimed that the addition of fins increased the PTCs' thermal efficiency. Reddy et al. [29] discovered that a PTC performs better when fins are designed in various geometric shapes, including triangular, square, circular, and trapezoidal. In an experimental setting, Ullah and Kang [30] evaluated the efficacy of parabolic sunray collectors in the drying process of seasonal fruits at different air flow rates. Their findings indicated that 3.50 kg/min and 1.5 kg/min air mass flow rates produced the highest and lowest mean efficiencies of 23% and 19.6%, respectively. When flow rates were at their highest, temperatures of 51 °C and 84 °C were recorded within the collector's drying chamber and absorber pipe, respectively. Zhao et al. [31] evaluated the overall PTSC performance for medium-temperature heat requirements with three receiver tubes of different structures. Air temperature increased by 266 °C under about 900 W/m² of sunray energy and an airflow rate of 93 Nm³/h. The energy and exergy efficiencies of the inside pin-finned tube were measured and found to be 10.4–14.5% and 2.55–4.29%, respectively, more significant than the energy and exergy efficiencies of the smooth tube across the airflow rate range examined. Chen et al. [32] demonstrated an innovative multi-surface sunray collector with double receiver tubes. Experimental results showed that the innovative collector met 11% to 81% of the heat demand from December to January, resulting in an active heat gain of 11,831 GJ. Table 1 shows studies that enhance heat transfer in parabolic trough air heating applications. Salman et al. [33] investigated the effect of the flow and geometric parameters of a dimple-roughened absorber plate on the enactment of solar air collectors (SACs) with air-impinging jets. Khargotra et al. [34] focused on the design and optimization of a solar water heating system (SWHS) integrated with perforated delta obstacles. Investigation and optimization were performed regarding the effects of the Reynolds number, angle of attack, and pitch ratio on the thermo-hydraulic performance, friction factor, and Nusselt number. The analytic hierarchy process-additive ratio assessment method of multicriteria decision making was used.

In this regard, the thermal performance of a parabolic solar air collector for low- and medium-temperature applications was experimentally tested in an outdoor environment. Although the idea of PTAC is well known in the current body of literature and many tests of PTAC have been investigated by researchers, two things are still missing:

- First, the inclusion of a heat exchanger and a helical strip inside an evacuated tube open at one end has not been tested experimentally yet.

- Second, alternatives to the evacuated tube that give the same or more performance remain to be found.

Table 1. List of recent investigations of the parabolic trough air collector (PTAC) thermal enhancement technique.

Experiment	Method	Sunray System	Sunray Insolation	Air Outlet Temperature	Thermal Efficiency
			W/m ²	°C	%
Mwesigye et al. [35]	THE	PTAC system with twisted tape	-	129	~70
Bellos et al. [36]	THE	PTAC system, with tube and longitudinal fin	800	590	61.4
Nemš et al. [37]	THE & EXP	PTAC system with an internal multiple-fin array	1008	79.4	42
Pandey et al. [38]	THE & EXP	PTAC system with Evacuated tube and U-tube copper pipe	~1100	151	28.8

EXP: experimental, THE: theoretical, and THE & EXP: theoretical and experimental.

The present study aimed to enrich the field of research in parabolic trough air heating systems. The following points were implemented to accomplish the chief objective.

1. To improve the heat transfer performance, a spiral strip and a heat exchanger were designed and installed along the path of the airflow inside the evacuated tube.
2. Spiral strips increased the path of fluid flow, thus increasing the rate of heat transfer.
3. To monitor the impact, the PTAC system was tested and an evacuated tube and the results were measured (case 1).
4. Design and installation of a new cavity receiver and several arranged quadrangular pyramidal elements were performed and tested experimentally (case 2).

As a result, it is anticipated that this study will significantly contribute to improving the heat transmission of PTAC systems.

2. Materials and Methods

The performance of the parabolic trough air collector PTAC is significantly influenced by the surrounding environment. The solar energy research site located at the University of Technology building in Baghdad, Iraq was chosen for the installation of the PTAC model. This location has a latitude of 33°18'46.0980" N, 44°21'41.3568" E.

As mentioned previously, the PTAC model consists of a frame, reflector, evacuated tube receiver, cavity receiver, blower, and measuring instruments. The next section contains a description of the conceptual design scheme for the PTAC. The process flow chart in Figure 1 represents the research methodology applied in this study.

2.1. Optimum Optical Efficiency

This section details the various designs proposed for the parabolic trough. A parabolic trough collector was simulated in a ray optics simulation platform. The idea to develop a PTC with important geometrical parameters in order to improve the geometric concentration ratio was put into practice. A parabolic trough collector was simulated on a fixed focal line of 2 m, with a variable aperture area from 1 m to 2 m and a 10-cm-width receiver on the trough focal line; a ray tracer was used to compute the path of the rays. The simulation was performed under the assumption that the trough was perfectly oriented and the rays were parallel. Afterward, all the rays were focused on the focal line. Figure 2 lists the specifications of the path states of the focused sunray radiation hitting the focal line at different dimensions of the parabolic trough. The figure also shows the trough efficiency (proportional to the rays reaching the absorber) concerning the shape of the trough and considering all the similarities between the rays.

It can be seen from Figure 2 that each (a2, b2, c2 and d2) has the fewest optical losses due to the focus of all the focused radiation beams being toward the receiver. Taking economic needs and the research requirements into consideration, design b was chosen, with a focal length of 460 mm. The parabolic trough collector system contains a trough with an aperture area (1200 mm × 2000 mm) oriented from south to north, as shown in Figure 3.

A trough is arranged so that heat transfer fluid (HTF) gradually acquires heat while it passes through the tubes. PTSC mainly comprises a reflector, a receiver, a supporting structure, and a tracking system. The parabola-shaped reflector, specially designed for concentrating sunray applications with high reflectivity (80%), will help to concentrate incoming sunrays to a tube placed along the middle of the trough.

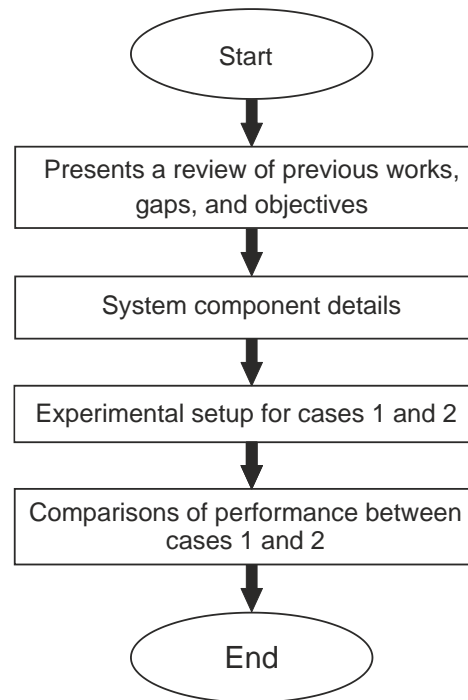


Figure 1. Description of the flowchart for the current study.

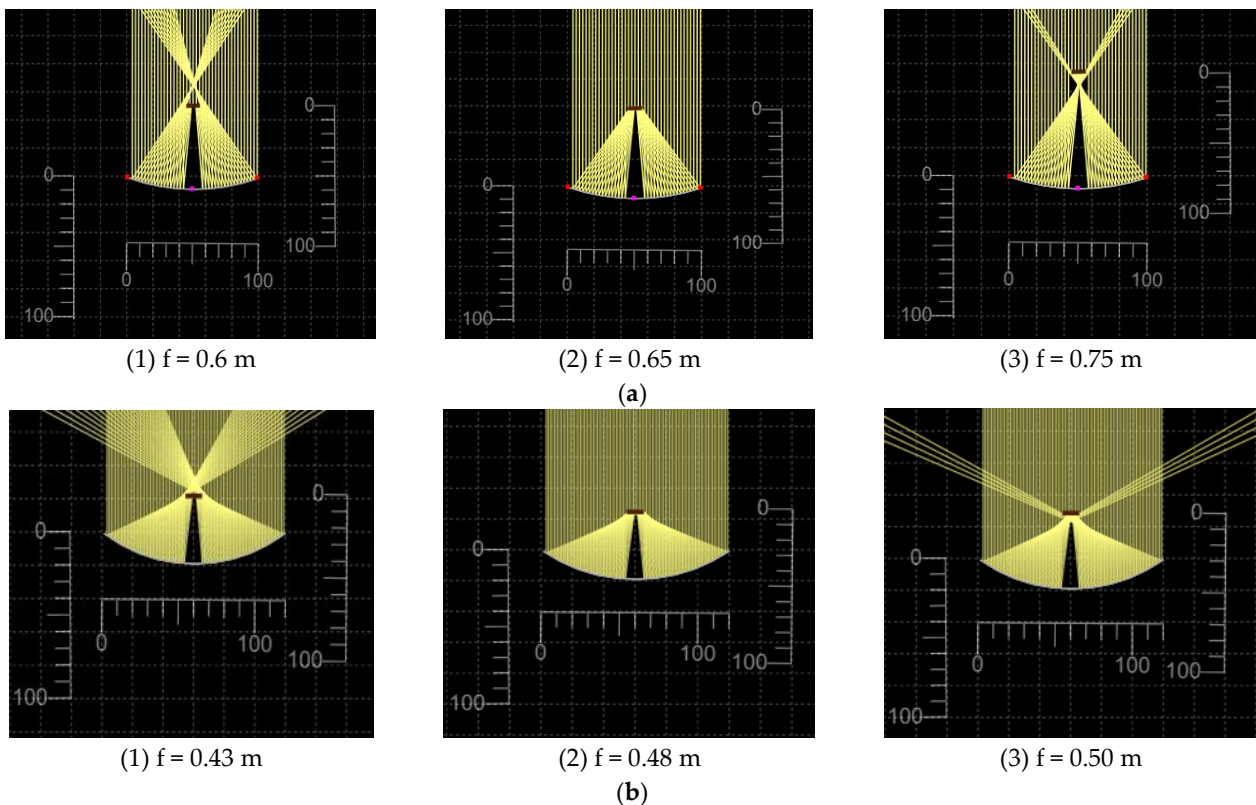


Figure 2. Cont.

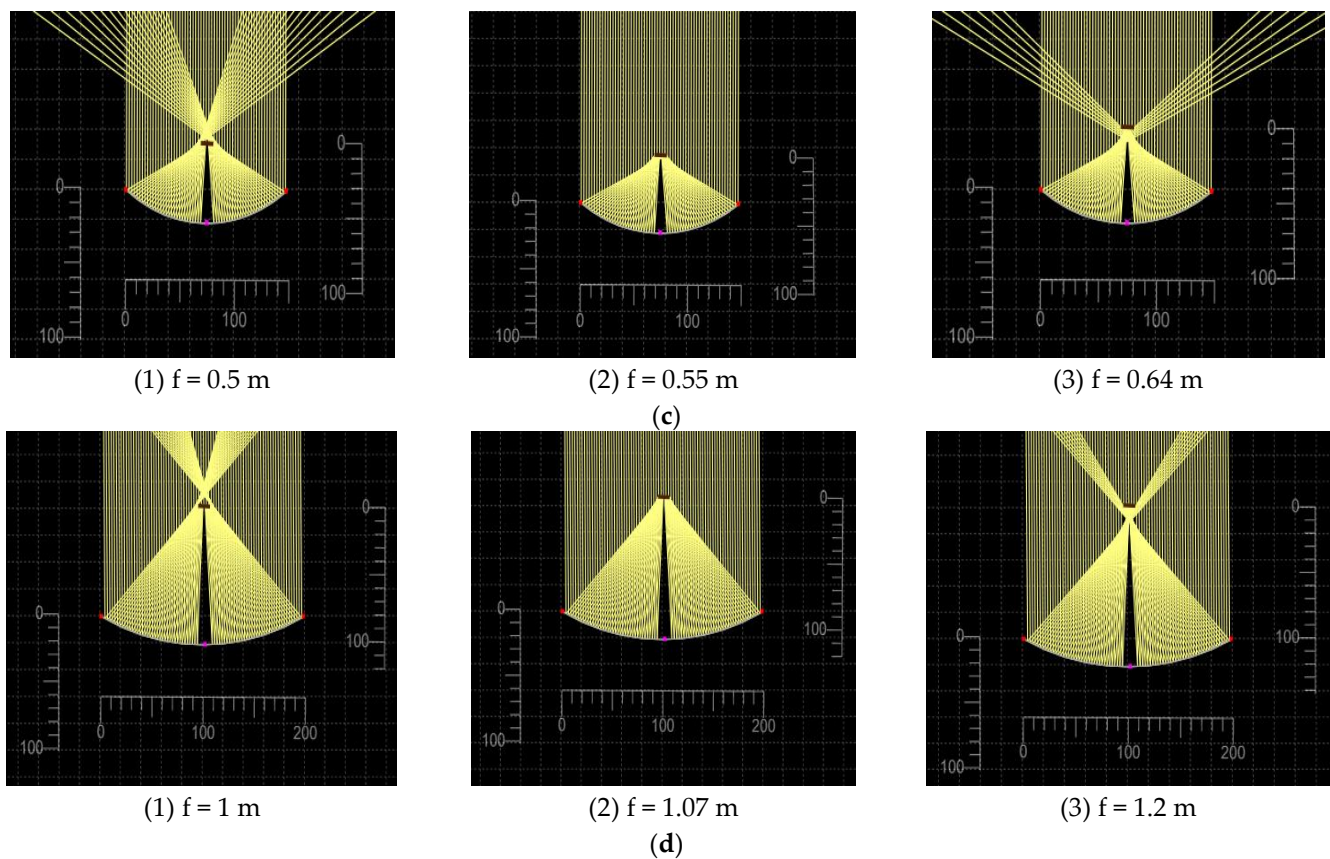


Figure 2. Circular mirrors are used to focus parallel rays of light with different rim angles: (a) Trough width = 1 m and trough depth = 0.1 m, (b) Trough width = 1.2 m and trough depth = 0.2 m, (c) Trough width = 1.5 m and trough depth = 0.25 m, (d) Trough width = 2 m and trough depth = 0.2 m.

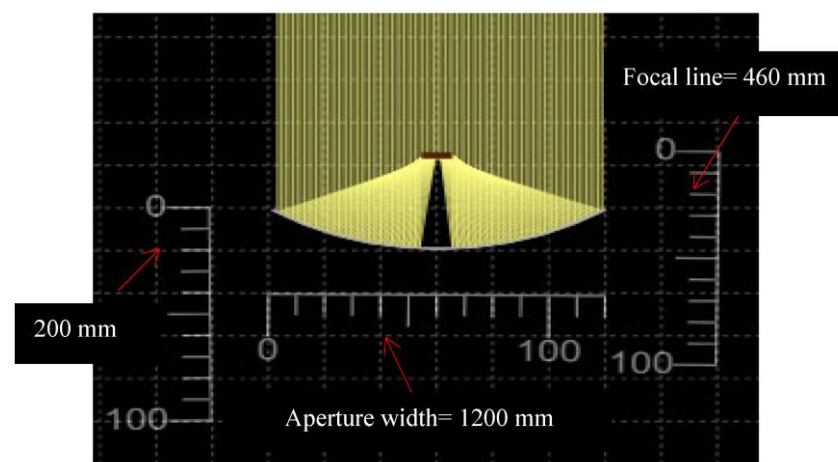


Figure 3. The proposed parabolic trough collector structure.

2.2. Experimental Setup and Procedure

A polished aluminum sheet with high reflectivity and low absorption rate was used as a parabolic reflector. The one-piece reflector plate has a length, aperture width, and thickness of 2000, 1200, and 4 mm, respectively. A 3.70 mm foam was attached to the board back for strength and to simplify mounting the board to the reflector bed with a parabolic shape. Consequently, the 4 mm thin aluminum plate was shielded from damage throughout installation, allowing for significant flexibility and making transportation markedly easy.

The receiver was mounted along the reflector's central axis to obtain focused sunray radiation and convert this to heat energy. The experimental setup was positioned facing the south in the east-west direction and tracking the sun from south to north. Table 2 presents the complete technical data sheet for the sunray collector.

Table 2. Sunray collector data.

Concentrator	Profile	Parabolic
	Rim angle	80°
	Focal length	460 mm
	Reflectivity of mirror	0.80
	Mirror plate material	PMMA, 4 mm
	Reflector layer	Aluminium (rear side)
	Aperture width	1200 m
	Length	2000 mm

2.3. Design Details of the Investigated Receiver Tubes/Cavity

Two different types of receivers were proposed to be investigated. Accordingly, the design and fabrication of the two types of receivers (insertion of a tube with a spiral strip into the evacuated tube (case 1) and a pyramidal cavity receiver (case 2)) were carried out and are presented in this section. Detailed descriptions of the receivers are also presented.

2.4. Modification Made in the Evacuated Tube Receiver (Case 1)

In this investigation, the evacuated tube from a traditional sunray water heater was modified and utilized as a receiver tube in the parabolic trough. Table 3 lists the requirements for the evacuated tube. This tube comprises two high-chemical and thermal-strength borosilicate glass tubes in which a sputtered sunray selective layer covers the exterior surface of the inner diameter. The sunray heat pipe's inner and outer tubes are bonded together. The annular area between the outer and inner tubes is vacuumed to eliminate heat losses. The evacuated receiver tube has two apertures to provide a separate entrance and outflow of the fluid from the tube. A T-type valve system was created for this purpose. The fluid enters perpendicular to the evacuated tube axis and departs parallel to the tube through a valve. The modified evacuated tube used in the tests is shown in Figure 4. The valve contains a spiral strip that impedes the movement of the working fluid and thus increases heat gain, as shown in Figure 5. At a later time, air can be collected from the tube.

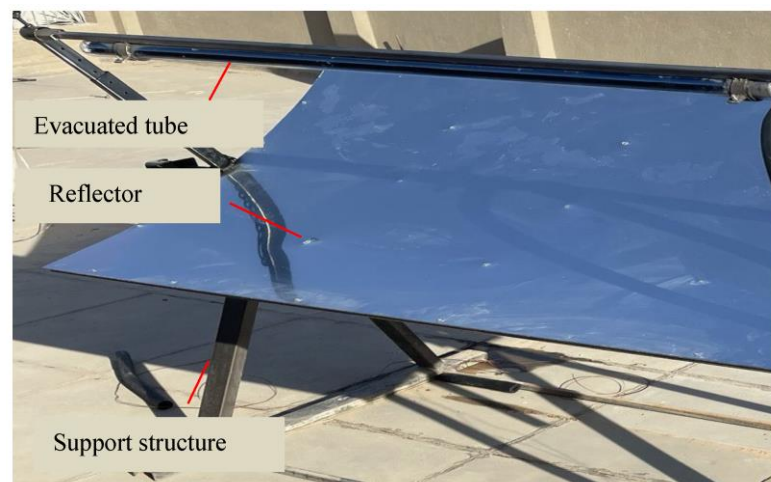
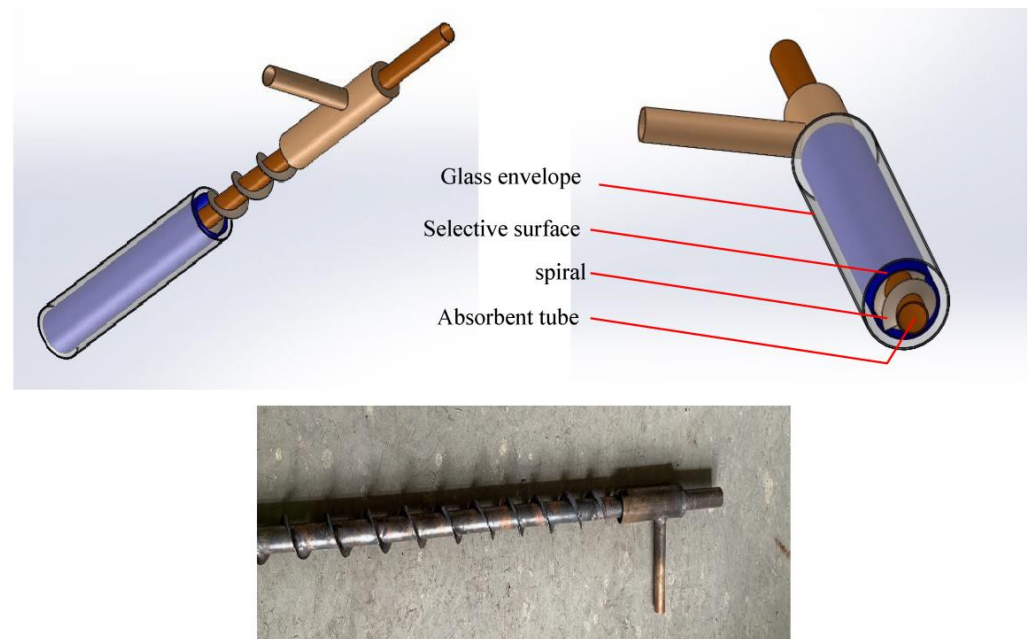


Figure 4. Concentrating the sunray collector with the evacuated tube receiver.

Table 3. Technical data for the evacuated tube.

Evacuated Tube Receiver	Glass Material	Borosilicate Glass 3.3
	Coating type	ALN/AIN-SS/Cu (aluminium nitride, AIN-SS, copper)
	Absorptance, α	≥ 0.94
	Emission ratio, ε	≤ 0.06
	Sunray transmission rate, τ	$\geq 92\%$
	Glazing outer and inner diameter (mm)	59, 43 mm
	The diameter of the helix	37 mm
	Length of the tube, L_g (mm)	1830 mm

**Figure 5.** Evacuated tube with a spiral strip.

2.5. Triangular Receiver Cavity Design (Case 2)

The new receiver is modular and scalable because it comprises separate components. The new design's purpose is to limit heat loss, mainly through engineering that prevents radiative losses from reaching the atmosphere. The new receiver consists of several pyramidal square elements arranged vertically, pointing to a parabolic trough. The working fluid in the passages behind the heating surfaces absorbs the concentrated sunray radiations reflected on the cavity's heating surface. Many researchers globally have worked on various designs for receiver cavities [39,40]. To date, the triangular cavity has been found to have the best optical and thermal performance, resulting in the geometry of the cavity being considered in this study. The proposed triangle receiver cavity design includes two rectangular plates with a tiny aperture. Two heating plates are employed on the interior of the cavity at an 80° angle to one another. Rectangular fins are supplied on the backside of the heating plates to improve heat transmission between the working fluid and the heating plate. They are laid horizontally and made of thin flat metal sheets, allowing heat to be transported from the front surface of the receiver through the fin body and efficiently released into the working fluid, as shown in Figure 6. The fins' efficiency can be improved through choosing the most suitable materials for the study on the basis of temperature. Experiments were conducted on variable parameters, like mass flow rate and sunray radiation. Insulation was added to the receiver chamber's rear side to reduce heat loss. Figure 7 shows the cavity receiver image, and Table 4 presents a thorough technical data sheet for the cavity receiver. Table 5 provides a list of the measuring equipment and measurement precision parameters.

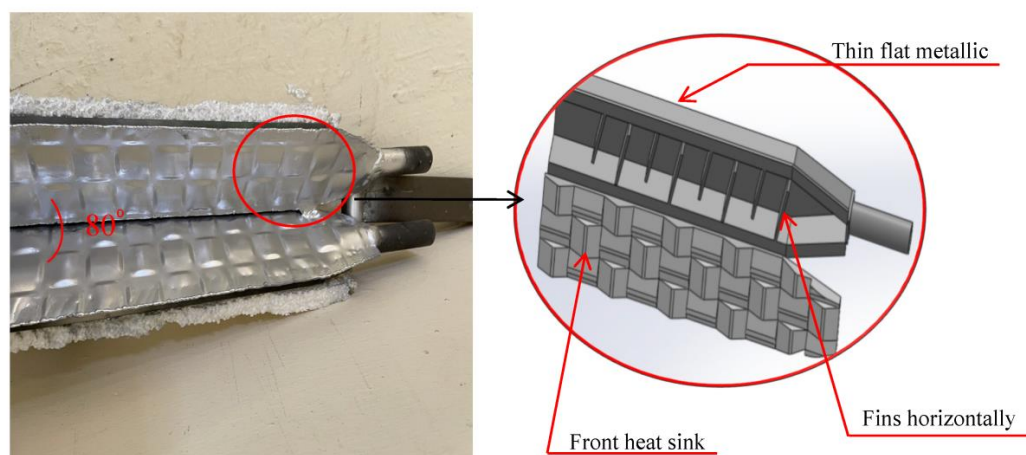


Figure 6. The cavity receiver with horizontal fins made of thin flat sheet metal.

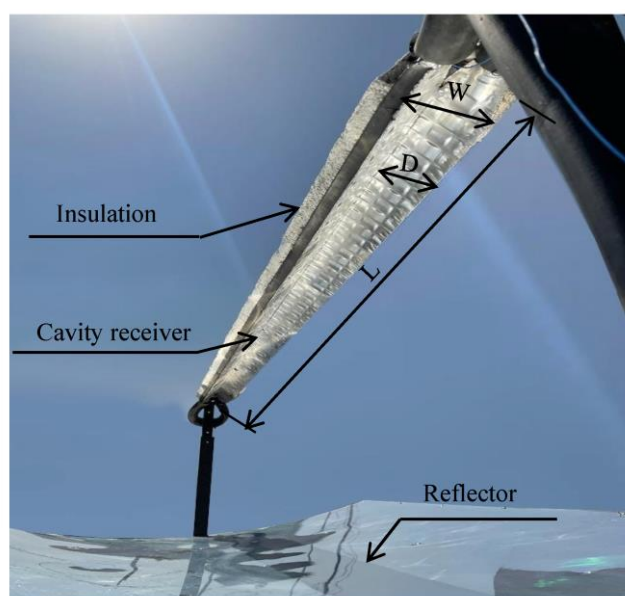


Figure 7. The concentrated sunray collector with cavity receiver as air heater.

Table 4. Technical data for the cavity receiver.

Receiver Cavity	Material	stainless steel
	Aperture Width, D	100 mm
	Absorber Plate Width, W	50 mm
	Absorber Plate Thickness, p	1.5 mm
	Inscribed Angle, θ	80°
	Absorber Length, L	1830 mm
	Fin length	40 mm
	Fin depth	15 mm
	Fin width	1 mm
	Space between fins	80 mm
	Number of rows of fins, N	20

Table 5. Specifications of the measuring instruments.

Device	Measuring Parameters	Range	Accuracy
Pyranometer	Global Radiation	0–2000 W/m ²	±5%
K-type thermocouple	Temperature	0–200 °C	±2%
Anemometer	Air velocity	0.4–30 m/s	±(2% + 0.2 m/s)

3. Analysis of the Thermal Performance of the PTAC

In this section, formulas for evaluating the energy and thermal-hydraulic performance of a PTAC are offered. It is assumed that quasi-steady state circumstances will be present for the performance assessment of the PTAC.

3.1. Energy Analysis

This section explains how to calculate the energy performance of a PTAC. The performance of the PTAC is assessed in quasi-stable conditions, according to ASTM E905-87-Standard Examination Technique for Determination of Thermal Efficiency of Tracked Concentrated Sunray Collectors (CSP).

The useful heat transfer rate (Q_u) that is transported to the process air in the absorption tube is found using the following equation [31]:

$$Q_u = \dot{m} \times (C_{p.T_{out}} \times T_{out} - C_{p.T_{in}} \times T_{in}) \quad (1)$$

where T_{in} is the air temperature at the inlet of the receiver ($^{\circ}\text{C}$) and T_{out} is the air temperature at the outlet of the receiver ($^{\circ}\text{C}$), the air mass flow rate is denoted by \dot{m} , and C_p denotes air-specific heat, which can be seen as a continuous function of temperature if curve fitting is applied:

$$C_p(T) = 1050 - 0.365T + 0.85 \times 10^{-3}T^2 - 0.39 \times 10^{-6}T^3 \quad (2)$$

The overall PTAC thermal efficiency is determined as follows [31]: The collector's usable energy to sunray energy ratio arrives at the parabolic reflector simultaneously:

$$\eta = \frac{Q_u}{Q_s} = \frac{\int_{T_1}^{T_2} \dot{m} \times (C_{p.T_{out}} \times T_{out} - C_{p.T_{in}} \times T_{in}) d\tau}{\int_{T_1}^{T_2} A_{ap} \cdot DNI d\tau} \quad (3)$$

$$Q_s = A_{ap} \cdot DNI \quad (4)$$

where A_{ap} is collector aperture area (m^2).

3.2. Thermal-Hydraulic Analysis

The following Kasperski-proposed equation can be used to determine the thermal-hydraulic efficiency of the PTAC [41].

$$\eta_{t-h} = \frac{V\rho C_p(T_{out} - T_{in}) - V\Delta P/\eta_{blw}}{A_{ap}DNI} \quad (5)$$

where the blower efficiency (η_{blw}) is deduced to be 0.65 in terms of the blower characteristics, ΔP is the pressure difference, ρ is the air density, and V is the volumetric flux. Here the aperture area (A_{ap}) and the radiation hitting the surface (DNI) are indicated.

3.3. Uncertainty Analysis

To assess the reliability of the PTAC experimental apparatus, an uncertainty analysis was performed. Examples of parameters that can be immediately observed include temperature and DNI. These data are shown in Table 2 along with the uncertainty ranges of the measurement instruments. The following formula is used to determine the receiver efficiency's uncertainty estimate [42].

$$\Delta\eta = \sqrt{\left(\Delta V \frac{\partial\eta_{rec}}{\partial V} + \Delta T_{out} \frac{\partial\eta_{rec}}{\partial T_{out}} + \Delta T_{in} \frac{\partial\eta_{rec}}{\partial T_{in}} + \Delta DNI \frac{\partial\eta_{rec}}{\partial DNI} \right)^2} \quad (6)$$

Accordingly, the predicted uncertainty of the receiver efficiency for the cases was within the range of $\pm 7.2\%$.

4. Results and Discussion

The tests were conducted at the Science and Technology Research Center at the University of Technology, Baghdad, Iraq (33°18'46.0980" N, 44°21'41.3568" E) during the month of March from 11:00 a.m. to 1:00 p.m. The outcomes of the external tests are assessed in this section. In particular, 0.0105 and 0.021 kg/s inlet air flow rates were used to compare the system performance characteristics of an evacuated tube with a spiral strip copper tube inside (case 1) and a cavity receiver with a hierarchical square surface (case 2), with variable radiation intensity and mass flow rate.

4.1. Temperature Evaluation

The experiment aimed to compare thermal performances between cases 1 and 2 and determine if a correlation exists between temperature increase and sunray radiation. The temperature at the collector's input is highly reliant on ambient temperature since the system does not function in a closed cycle. A portion of the information gathered during testing from 11:00 a.m. to 1:00 p.m. indicates that a beam shift irradiation influences the ambient temperature increase from 26 to 34 °C from 590 W/m² to 850 W/m². According to regression lines, temperature increase and sun irradiation have a nearly linear relationship. The sunray radiation intensity and atmospheric/ambient air temperature were measured for two hours. These factors may change regularly due to meteorological conditions, thereby impacting the performance of the experimental setup.

Figures 8–11 show the experiments' total results, including instantaneously sunray energy levels and temperature on typical days. The test values are plotted for a day with a clear sky, as shown in Figures 8 and 9. Temperature and DNI are measured at 5 min intervals. Figures 8 and 9 show the main parameters recorded during the tests of cases 1 and 2 for sunny days. The results were monitored from 11:00 to 13:00. Air flow rate remained constant at 0.0105 kg/s. Note that variations in DNI (<220 W/m²) have a limited effect on output temperatures.

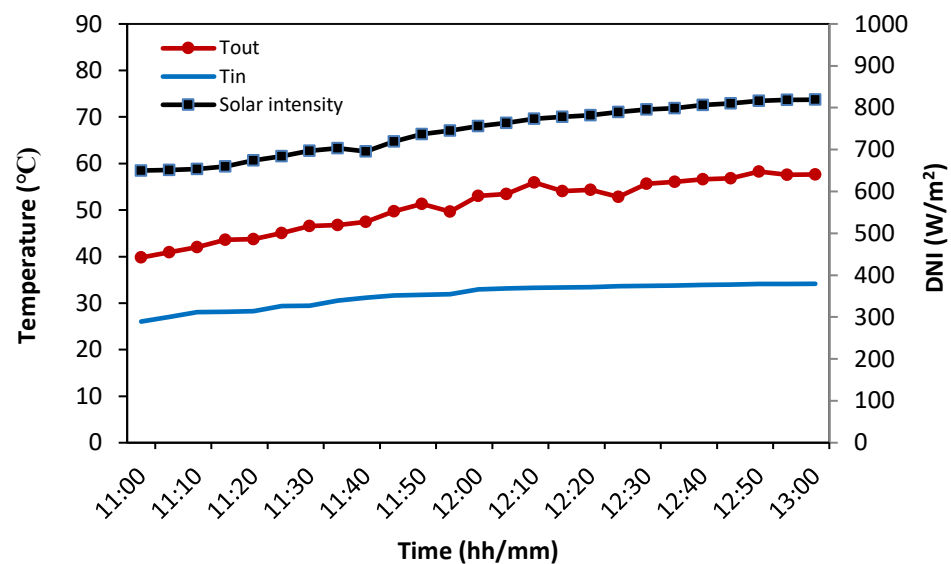


Figure 8. Air temperatures of the inlet and outlet for the absorber tube and DNI case 1 under the mass flow rate 0.0105 kg/s.

Given that the airflow rate in the PTACs remained constant and no air was circulated, temperature increases across PTACs could be directly compared when determining collector performance. Temperature increases were 58.2 °C and 55.6 °C in cases 1 and 2, respectively. In addition, the temperature increase was 4% higher in case 1 than in case 2, whereas the effective DNI was 3% less in case 1 than in case 2. Convergence between cases 1 and 2 in increasing the temperature is remarkable as a result of the proposed design in case 2, which

is represented in the role of hierarchical square surfaces in increasing the area of exposure to concentrated sunray radiation, thereby approximating the performance of case 1. As shown in Figures 8 and 9, as the day passes, the intensity of sunray radiation rises, and ambient air temperature follows the same trend. Over time, the amount of sunlight absorbed by the Earth increases, thereby increasing the surrounding air temperature. The intensity of sunray radiation increases and peaks at 819 W/m^2 and 845 W/m^2 for cases 1 and 2, respectively, at around 13:00.

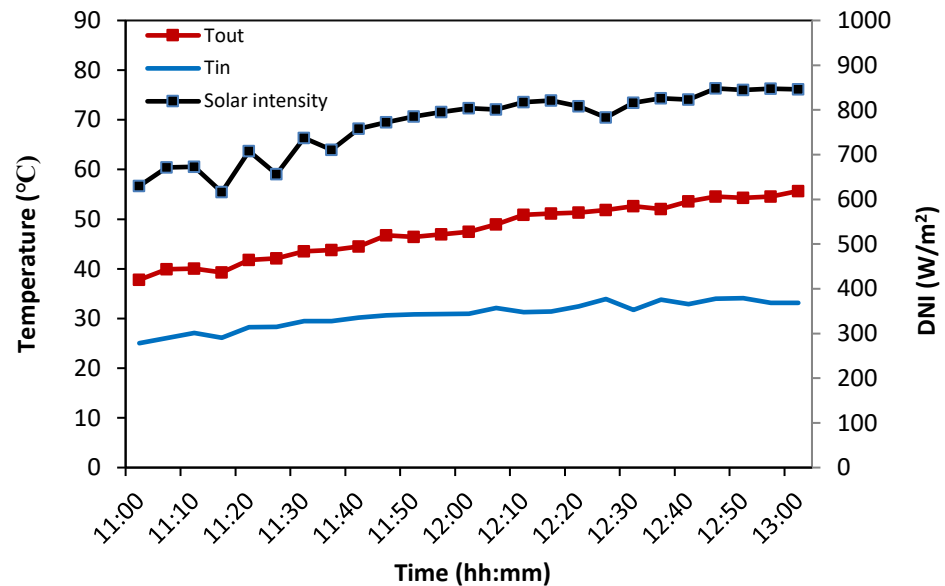


Figure 9. Air temperatures of the inlet and outlet for the absorber tube and DNI case 2 under the mass flow rate 0.0105 kg/s .

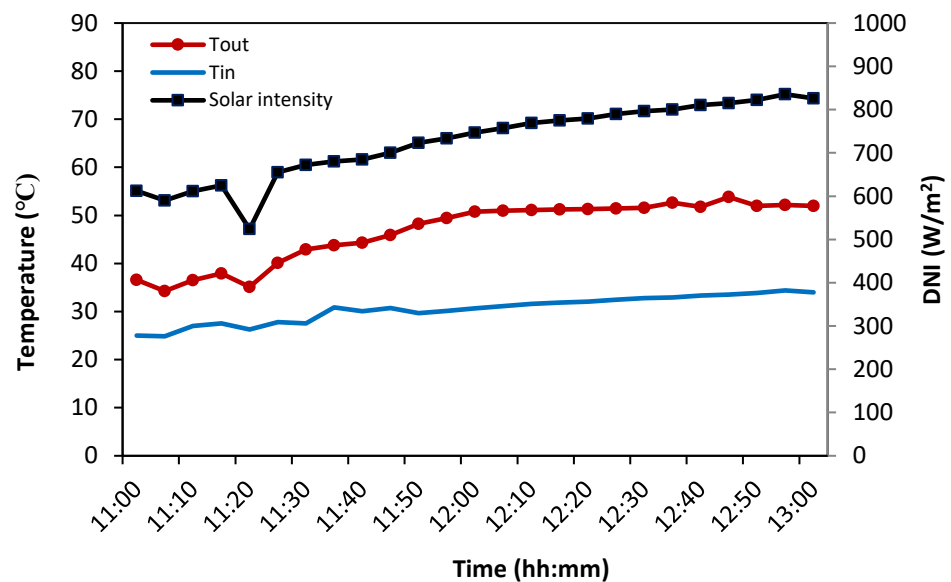


Figure 10. Temperatures of inlet and outlet air for the absorber tube and DNI case 1 under the mass flow rate of 0.021 kg/s .

As shown in Figures 10 and 11, the obtained output air temperatures corresponding to the system are calculated from the tests performed for cases 1 and 2 at a constant air intake flow rate of 0.021 kg/s , and different radiation rates are given. Note that the air leaving the receiver temperature is lower in cases 1 and 2 at 0.021 kg/s compared with that

of 0.0105 kg/s. Outlet air temperatures were 53.8 °C and 50 °C in the tests performed for cases 1 and 2, respectively, at the same inlet air flow rate.

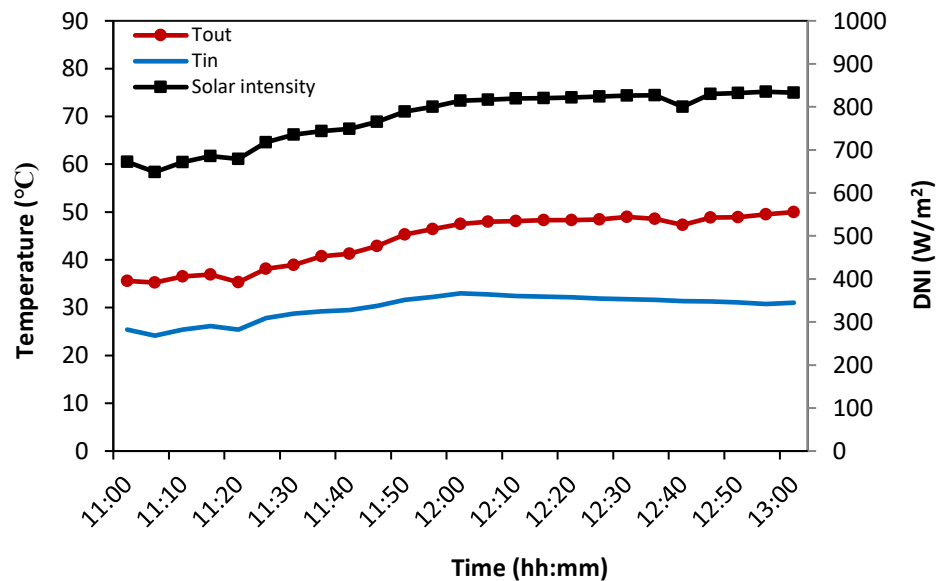


Figure 11. Temperatures of inlet and outlet air for the absorber tube and DNI case 2 under the mass flow rate of 0.021 kg/s.

The temperature derived from PTAC data collected under different irradiation conditions and at rates of 0.0105 kg/s and 0.021 kg/s is presented in Figures 8–11. Given that for approximately the same sunray radiation intensity more air must be heated, the outlet temperature of both systems with high airflow rates was lower than that with low airflow rates. For cases 1 and 2, the percentage decreases in temperature for the 0.021 kg/s flow rate compared with the 0.0105 kg/s flow rate were 7.5% and 10%, respectively.

4.2. Energy Analysis for a Mass Flow Rate of 0.0105 kg/s

Figures 12–14 depict the trial results, including instantaneous temperature change and sun energy levels. The airflow rate was maintained at a consistent rate of 0.0105 kg/s. In addition, experimental data were presented for the corresponding temperature evolution within the evacuated tube receiver and cavity receiver at various irradiation levels. The results of the tests performed under variable sunray irradiance, using an evacuated tube, a spiral tape (case 1), and a cavity receiver (case 2) and evaluated concerning the parabolic collector outlet temperatures obtained in the experiments are shown in Figure 12. The data show that as the intensity of the radiation increases, so does the temperature of the surrounding air. For example, under the same conditions of sunray radiation 844 W/m², we find that the outlet temperatures of the receiver are 58 °C and 54 °C in cases 1 and 2, respectively. Although employing a helical tape hinders the airflow and enables the airflow to spend more time in the absorber, adopting the new receiver design (case 2) brings the output temperature closer to case 1, in which the difference is merely 4 °C.

Air with a flow rate of 0.0105 kg/s was delivered to both exchangers to determine the temperature difference obtained, one after the other. In a similar experimental setup, the maximum/outlet temperature of the case 1 and case 2 heat exchangers was monitored over two hours. The temperature difference rose with increasing sunray radiation for both heat exchangers, as illustrated in Figure 13. Due to the vacuum, which limits heat loss, the temperature difference in case 1 was continuously more significant than in case 2; the spiral strip increases the air path, thereby increasing absorption. The temperature difference for the initially lower temperature ranges was 8% higher for case 1 than for case 2. However, the percentage increase was only 14.2% in the noon peak hours.

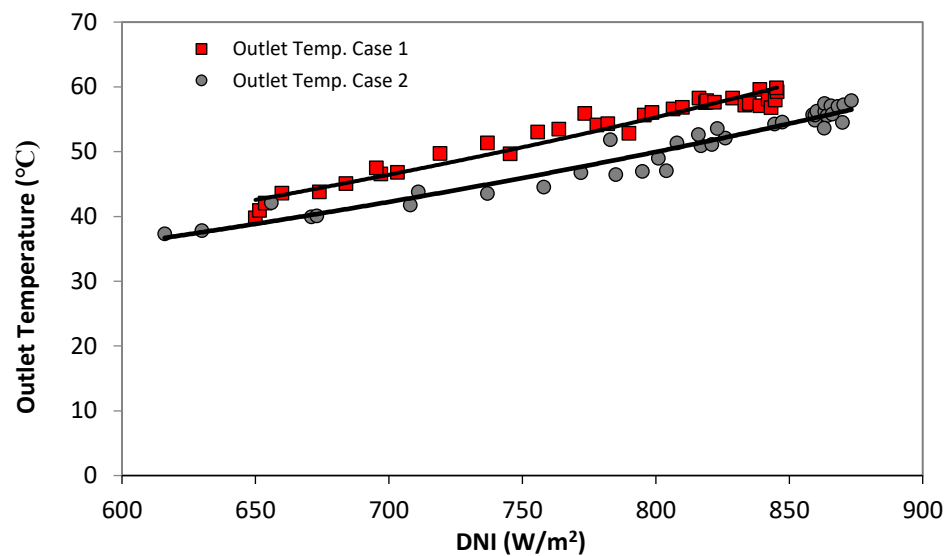


Figure 12. Variation in outside air temperature with sunray radiation (0.0105 kg/s).

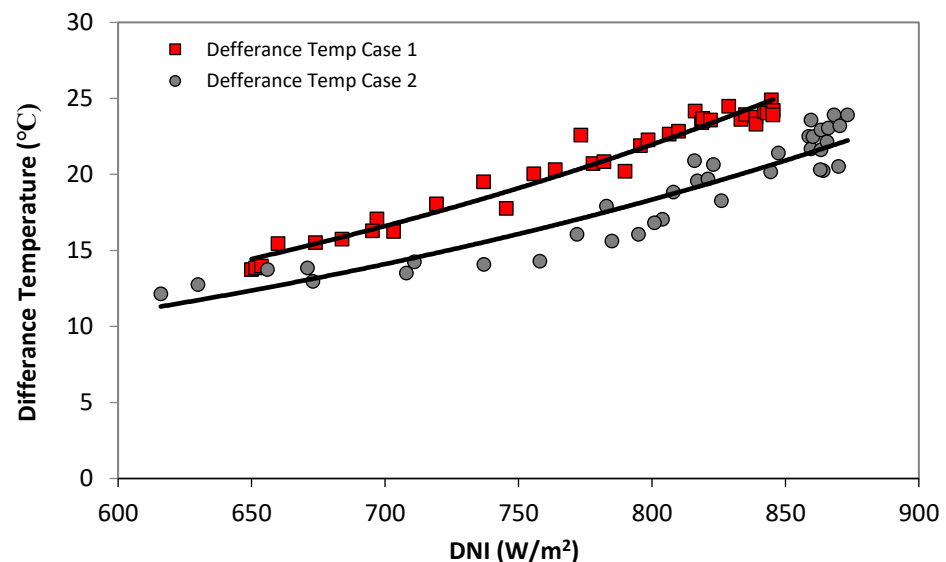


Figure 13. Variation in difference temperature with sunray radiation (0.0105 kg/s).

Figure 14 depicts the influence of the temperature differential between input and output air on thermal efficiency for various sunray radiation levels. With the case 1 heat exchanger, the sunray air heater efficiency increased from 9.3% to 10.8% and remained nearly constant. With an increase from 8.2% to 9.4% in efficiency variance, the case 2 heat exchanger followed the same trend. The fact that the efficacy of a sunray air heater is proportional to the temperature differential between the exit and intake air explains this tendency. Figure 14 further shows that when the highest temperature difference was 23.6 °C, the maximum efficiency of the air heater with the heat exchanger in cases 1 and 2 varied by 13%, while the difference became minimal at 14 °C, which is 12.6%. Despite increasing pressure losses in the system due to the absorbent tube with spiral strip being inserted with various radiances and a constant air flow rate, the system becomes ideal due to the enhanced thermal efficiency.

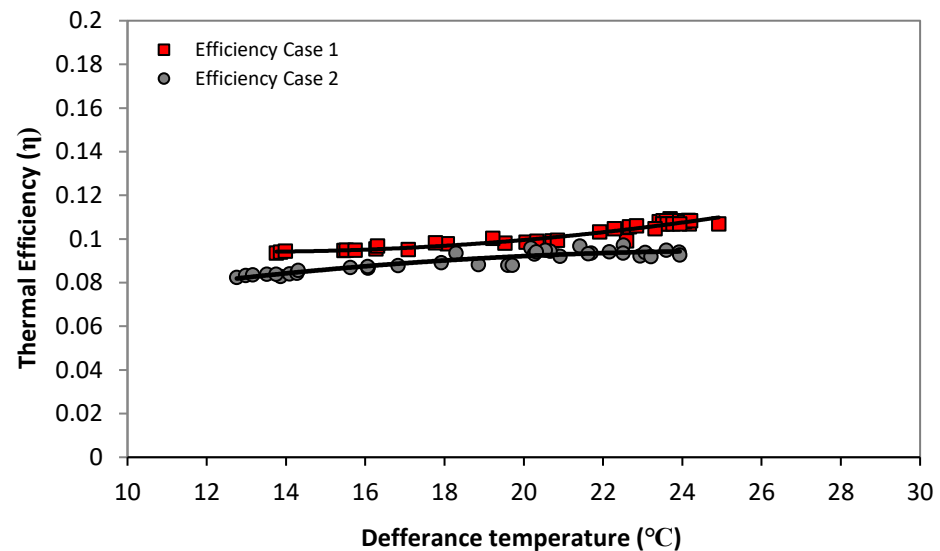


Figure 14. Variation in thermal efficiency with difference temperature (0.0105 kg/s).

4.3. Thermal-Hydraulic Efficiency

In this part, we tested thermal-hydraulic efficiency, which includes both thermal and hydraulic considerations and the pressure losses in the evacuated tube with helical screw inserts at different radiations. The reason why this mass flow rate was chosen is that the maximum thermal efficiencies were achieved under 0.021 kg/s. As shown in Figure 15, although the radiation intensity reduces the thermo-hydraulic efficiency, another factor that greatly influences the result is the presence of the spiral strip (case 1) and the horizontal fins of the cavity receiver (case 2), causing more pressure losses in the receiver.

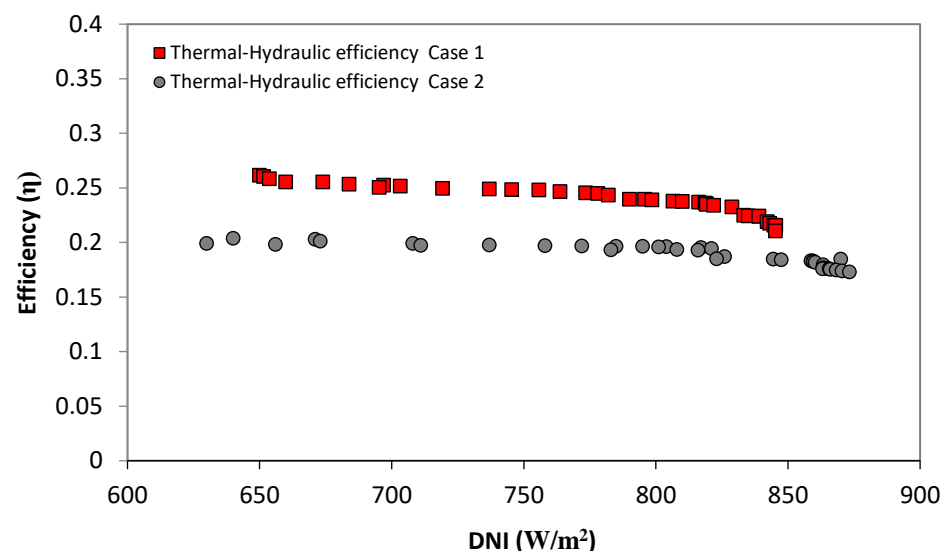


Figure 15. Variation in thermal-hydraulic efficiency with DNI (0.021 kg/s).

According to the experimental results, the pressure loss in the manifold tube with the spiral strip (case 1) was less than the cavity receiver with horizontal fins (case 2) as a result of the working fluid needing to change its path every time it passed through the fin, which increased the pressure loss. Therefore, the rate of increase in thermo-hydraulic efficiencies in case 1 was 21% higher than in case 2. Although cases 1 and 2 increased the pressure loss in the system, the system became ideal because of the enhanced thermal efficiency.

5. Comparative Study

The current study's findings were compared to those found in the literature for the recently studied evacuated sunray tube collectors with reflectors. In contrast to other PTAC investigations, this study is unusual because it develops a new type of PTAC using a cavity receiver to improve thermal performance and compares it to an evacuated absorber tube with a spiral stripe insert. Table 6 shows that the operational parameters (e.g., geometry, materials, design) considerably impacted the evacuated tube sunray air collectors' thermal efficiency and temperature increase. Thermal efficiency increased as the airflow rate increased, given a few thermal losses. Compared to similar systems operating in a similar air flow rate range, the tested evacuated tube with spiral strip showed thermal efficiency nearly equal to other systems despite this system's open-cycle operation.

Table 6. Comparing the current study with the optimal values for various improvements in the literature.

Reference	System Geometry	Sunray Insolation	Air Mass Flow Rate	Efficiency	Temperature Rise
		(W/m ²)	(kg/s)	(%)	(°C)
Yadav et al. [39]	• One evacuated absorber tube with both ends open.	1000	0.01018	14	16
Bakry et al. [40]	• Open-ended evacuated tube with centre copper tube.	880	0.0006	8.5	133
Nain et al. [43]	• An evacuated tube with one end open and a U-shaped copper heat exchanger.	836	0.00126	11.6	80
	• An evacuated tube with one end open and a U-shaped copper heat exchanger with fins.	875	0.00126	14.7	91.4
Current study	• An evacuated tube on one end contains a copper tube and a spiral strip.	844	0.0105	10.7	24.9
	• Receiver with many quadrilateral pyramid-shaped elements arranged.	844	0.0105	9.3	21.4

The receiver cavity created had efficient performance and remarkable efficiency in supplying hot air. The system tested with the fins showed a slightly lower thermal efficiency and a lower temperature difference when operating at lower radiation levels than sunlight.

6. Conclusions

In this study, the characteristics of the performance of the PTAC system for two types of receivers were compared. The first type consisted of an evacuated tube with an absorbent tube surrounded by a spiral strip (case 1), and the second type consisted of a cavity receiver with pyramidal square surfaces (case 2). Energy and thermal efficiency were evaluated using the absorber tube's inlet and outlet temperatures.

The conclusions are as follows:

- The findings indicate that the air temperature exiting the absorber tube is inversely related to the air input flow rate and directly proportional to the sunray radiation. Consequently, the most significant output air temperatures were attained at the lowest inlet flow rate and the highest sunray irradiation.
- Under the same sunray radiation conditions, the order of temperature increase of the heat transfer fluid was 39.7–58.2 °C and 37.8–55.6 °C for cases 1 and 2, respectively, at an inlet air flow rate of 0.0105 kg/s; and 34.2–53.82 °C and 35.6–50 °C for cases 1 and 2, respectively, at an inlet air flow rate of 0.021 kg/s.
- For both types of receivers, the temperature of the heat transfer fluid increase was tested for two hours for specific quantities of sunray energy. Cases 1 and 2 had thermal efficiency values of 9.3–10.8% and 8.2–9.4%, respectively, at an inlet air flow rate of 0.0105 kg/s.
- Based on observation, the bore cavity receiver with hierarchical square surfaces (case 2) resulted in a significant convergence of performance from the spiral strip inserted inside the evacuated tube (case 1) and was beneficial in the presence of designs for the sunray air collector.

- In future studies and according to the obtained results, the proposed receiver can be used as an alternative to the evacuated tube in the parabolic trough collector for medium- and high-temperature applications. This system can be also tested with various heat transfer fluids in other seasons of the year under other working conditions. In addition, the following factors should be considered, including pressure drop, friction, and pumping capacity.

Author Contributions: Conceptualization, A.K.K. and W.A.K.A.-M.; Methodology, A.K.K. and W.A.K.A.-M.; Validation, H.A.A.W.; Formal analysis, A.K.K.; Investigation, A.K.K. and H.A.A.W.; Data curation, W.A.K.A.-M., H.A.A.W. and F.A.; Writing—original draft, A.K.K., W.A.K.A.-M. and H.A.A.W.; Visualization, A.K.K., W.A.K.A.-M. and A.A.A.; Supervision, F.A. and B.E. All authors have read and agreed to the published version of the manuscript.

Funding: This research received no external funding.

Acknowledgments: We acknowledge the support of the Deutsche Forschungsgemeinschaft (DFG) German Research Foundation and the Open Access Publishing Fund of the Technical University of Darmstadt. The authors would also like to thank the University of Technology-Iraq.

Conflicts of Interest: All the authors certify that they have no affiliations or involvement with any organization or entity with any financial or nonfinancial interest in the subject or material discussed in this manuscript.

References

1. Khelif, A.K.; Gilani, S.I.U.H.; Al-Kayiem, H.H.; Mohammad, S.T. Concentrated sun ray tower hybrid evacuated tube-photovoltaic/thermal receiver with a non-imaging optic reflector: A case study. *J. Clean. Prod.* **2021**, *298*, 126683. [\[CrossRef\]](#)
2. Khafaji, H.Q.; Abdul, W.H.A.; Alsaedi, S.S.; Al-Maliki, W.A.K.; Alobaid, F.; Epple, B. Thermal performance evaluation of a tubular heat exchanger fitted with combined basket-twisted tape inserts. *Appl. Sci.* **2022**, *12*, 4807. [\[CrossRef\]](#)
3. Khafaji, H.Q.; Abdul, W.H.A.; Al-Maliki, W.A.K.; Alobaid, F.; Epple, B. Energy and Exergy Analysis for Single Slope Passive Solar Still with Different Water Depth Located in Baghdad Center. *Appl. Sci.* **2022**, *12*, 8561. [\[CrossRef\]](#)
4. Abdulhamed, A.J.; Adam, N.M.; Ab-Kadir, M.Z.A.; Hairuddin, A.A. Review of sun ray parabolic-trough collector geometrical and thermal analyses, performance, and applications. *Renew. Sustain. Energy Rev.* **2018**, *91*, 822–831. [\[CrossRef\]](#)
5. Njomo, D.; Daguene, M. Sensitivity analysis of thermal performances of flat plate sun ray air heaters. *Heat Mass Transf.* **2006**, *42*, 1065–1081. [\[CrossRef\]](#)
6. Wang, P.Y.; Guan, H.Y.; Liu, Z.H.; Wang, G.S.; Zhao, F.; Xiao, H.S. High temperature collecting performance of a new all-glass evacuated tubular sun ray air heater with a U-shaped tube heat exchanger. *Energy Convers. Manag.* **2014**, *77*, 315–323. [\[CrossRef\]](#)
7. Kumbhar, N.A.; Shinde, S.R.; Shinde, V.S. Performance investigation of parabolic trough sun ray collector integrated with thermal energy storage system. *Int. J. Curr. Eng. Technol.* **2016**, *5*, 424–430.
8. Al-Maliki, W.A.K.; Al-Hasnawi, A.G.T.; Abdul Wahhab, H.A.; Alobaid, F.; Epple, B. A Comparison Study on the Improved Operation Strategy for a Parabolic trough Solar Power Plant in Spain. *Appl. Sci.* **2021**, *119*, 576.
9. Al-Maliki, W.A.K.; Hadi, A.S.; Al-Khafaji, H.M.; Alobaid, F.; Epple, B. Dynamic Modelling and Advanced Process Control of Power Block for a Parabolic Trough Solar Power Plant. *Energies* **2022**, *151*, 29.
10. Çağlar, A. Design of a Parabolic trough Sun Ray Collector Using a Concentrator with High Reflectivity. In Proceedings of the 2nd World Congress on Mechanical, Chemical, and Material Engineering, Budapest, Hungary, 22–23 August 2016.
11. Kim, Y.; Seo, T. Thermal performance comparisons of the glass evacuated tube sun ray collectors with shapes of absorber tube. *Renew. Energy* **2007**, *32*, 772–795. [\[CrossRef\]](#)
12. Al-Maliki, W.A.K.; Alobaid, F.; Keil, A.; Epple, B. Dynamic Process Simulation of a Molten-Salt Energy Storage System. *Appl. Sci.* **2021**, *11*, 11308. [\[CrossRef\]](#)
13. Al-Maliki, W.A.K.; Khafaji, H.Q.; Abdul Wahhab, H.A.; Al-Khafaji, H.M.; Alobaid, F.; Epple, B. Advances in Process Modelling and Simulation of Parabolic Trough Power Plants: A Review. *Energies* **2022**, *15*, 5512. [\[CrossRef\]](#)
14. Ma, L.; Lu, Z.; Zhang, J.; Liang, R. Thermal performance analysis of the glass evacuated tube sun ray collector with U-tube. *Build. Environ.* **2010**, *45*, 1959–1967. [\[CrossRef\]](#)
15. Zinian, H.; Hongchuan, G.; Fulin, J.; Wei, L. A comparison of optical performance between evacuated collector tubes with flat and semicylindric absorbers. *Sun Ray Energy* **1997**, *60*, 109–117. [\[CrossRef\]](#)
16. Okonkwo, E.C.; Abid, M.; Ratlamwala, T.A. Numerical analysis of heat transfer enhancement in a parabolic trough collector based on geometry modifications and working fluid usage. *J. Sun Ray Energy Eng.* **2018**, *140*, 051009. [\[CrossRef\]](#)
17. Okonkwo, E.C.; Abid, M.; Ratlamwala, T.A. Comparative study of heat transfer enhancement in parabolic trough collector based on modified absorber geometry. *J. Energy Eng.* **2019**, *145*, 04019007. [\[CrossRef\]](#)
18. Demagh, Y.; Bordja, I.; Kabar, Y.; Benmoussa, H. A design method of an S-curved parabolic trough collector absorber with a three-dimensional heat flux density distribution. *Sun Ray Energy* **2015**, *122*, 873–884. [\[CrossRef\]](#)

19. Vishwakarma, S.; Debnath, K.; Debnath, B.K. Thermal performance study of helically grooved absorber tubes for parabolic trough sun ray collector. In Proceedings of the ASME Power Conference, Lake Buena Vista, FL, USA, 24–28 June 2018; Volume 51395, p. V001T06A009.
20. Al-Maliki, W.A.K.; Mahmoud, N.S.; Al-Khafaji, H.M.; Alobaid, F.; Epple, B. Design and Implementation of the Solar Field and Thermal Storage System Controllers for a Parabolic Trough Solar Power Plant. *Appl. Sci.* **2021**, *11*, 6155. [[CrossRef](#)]
21. Al-Maliki, W.A.K.; Hadi, A.S.; Al-Khafaji, H.M.; Alobaid, F.; Epple, B. Novel feedwater preheating system for parabolic trough solar power plant. *Energy Rep.* **2022**, *8*, 10665–10687. [[CrossRef](#)]
22. Al-Maliki, W.A.K.; Alobaid, F.; Starkloff, R.; Kez, V.; Epple, B. Investigation on the dynamic behaviour of a parabolic trough power plant during strongly cloudy days. *Appl. Therm. Eng.* **2016**, *99*, 114–132. [[CrossRef](#)]
23. Zou, B.; Dong, J.; Yao, Y.; Jiang, Y. An experimental investigation on a small-sized parabolic trough sun ray collector for water heating in cold areas. *Appl. Energy* **2016**, *163*, 396–407. [[CrossRef](#)]
24. Fuqiang, W.; Zhaxiang, T.; Xiangtao, G.; Jianyu, T.; Huaizhi, H.; Bingxi, L. Heat transfer performance enhancement and thermal strain restraint of tube receiver for parabolic trough sun ray collector by using asymmetric outward convex corrugated tube. *Energy* **2016**, *114*, 275–292. [[CrossRef](#)]
25. Zhang, L.; Yu, Z.; Fan, L.; Wang, W.; Chen, H.; Hu, Y.; Fan, J.; Ni, M.; Cen, K. An experimental investigation of the heat losses of a U-type sun ray heat pipe receiver of a parabolic trough collector-based natural circulation steam generation system. *Renew. Energy* **2013**, *57*, 262–268. [[CrossRef](#)]
26. Nain, S.; Parinam, A.; Kajal, S. Experimental study and analysis of air heating system using a parabolic trough sun ray collector. *Int. J. Ambient. Energy* **2018**, *39*, 143–146. [[CrossRef](#)]
27. Bellos, E.; Tzivanidis, C.; Tsimpoukis, D. Optimum number of internal fins in parabolic trough collectors. *Appl. Therm. Eng.* **2018**, *137*, 669–677. [[CrossRef](#)]
28. Muñoz, J.; Abánades, A. Analysis of internal helically finned tubes for parabolic trough design by CFD tools. *Appl. Energy* **2011**, *88*, 4139–4149. [[CrossRef](#)]
29. Reddy, K.S.; Satyanarayana, G.V. Numerical study of porous finned receiver for sun ray parabolic trough concentrator. *Eng. Appl. Comput. Fluid Mech.* **2008**, *2*, 172–184.
30. Ullah, F.; Kang, M. Impact of air flow rate on drying of apples and performance assessment of parabolic trough sun ray collector. *Appl. Therm. Eng.* **2017**, *127*, 275–280. [[CrossRef](#)]
31. Zhao, Z.; Bai, F.; Zhang, X.; Wang, Z. Experimental study of pin finned receiver tubes for a parabolic trough sun ray air collector. *Sun Ray Energy* **2020**, *207*, 91–102.
32. Chen, C.; Han, F.; Mahkamov, K.; Wei, S.; Ma, X.; Ling, H.; Zhao, C. Numerical and experimental study of laboratory and full-scale prototypes of the novel sun ray multi-surface air collector with double-receiver tubes integrated into a greenhouse heating system. *Sun Ray Energy* **2020**, *202*, 86–103.
33. Salman, M.; Chauhan, R.; Singh, T.; Prabakaran, R.; Kim, S.C. Experimental investigation and optimization of dimple-roughened impinging jet solar air collector using a novel AHP-MABAC approach. *Environ. Sci. Pollut. Res.* **2023**, *30*, 36259–36275. [[CrossRef](#)]
34. Khargotra, R.; Kumar, R.; Sharma, A.; Singh, T. Design and performance optimization of solar water heating system with perforated obstacle using hybrid multi-criteria decision-making approach. *J. Energy Storage* **2023**, *63*, 107099. [[CrossRef](#)]
35. Mwesigye, A.; Bello-Ochende, T.; Meyer, J.P. Heat transfer and entropy generation in a parabolic trough receiver with wall-detached twisted tape inserts. *Int. J. Therm. Sci.* **2016**, *99*, 238–257. [[CrossRef](#)]
36. Bellos, E.; Tzivanidis, C.; Daniil, I.; Antonopoulos, K.A. The impact of internal longitudinal fins in parabolic trough collectors operating with gases. *Energy Convers. Manag.* **2017**, *135*, 35–54. [[CrossRef](#)]
37. Nemš, M.; Kasperski, J. Experimental investigation of concentrated sun ray air-heater with internal multiple-fin array. *Renew. Energy* **2016**, *97*, 722–730. [[CrossRef](#)]
38. Pandey, S.; Mishra, S.K.; Sharma, A.; Verma, A.K.; Yadav, L. Performance analysis of evacuated tube type sun ray air heater with parabolic trough type collector. *Int. J. Energy Water Resour.* **2022**, *6*, 337–351. [[CrossRef](#)]
39. Yadav, A.; Kumar, M. Experimental study and analysis of parabolic trough collector with various reflectors. *Int. J. Energy Power Eng.* **2013**, *7*, 1659–1663.
40. Bakry, A.I.; El-Samadony, Y.A.F.; El-Agouz, S.A.; Alshrombably, A.M.; Abdelfatah, K.S.; Said, M.A. Performance of the one-ended evacuated tubes as medium temperature sun ray air heaters at low flow rates. *Sustain. Energy Technol. Assess.* **2018**, *30*, 174–182.
41. Kasperski, J.; Nemš, M. Investigation of thermo-hydraulic performance of concentrated solar air-heater with internal multiple-fin array. *Appl. Therm. Eng.* **2013**, *58*, 411–419. [[CrossRef](#)]
42. Fernández-García, A.; Valenzuela, L.; Zarza, E.; Rojas, E.; Pérez, M.; Hernández-Escobedo, Q.; Manzano-Agugliaro, F. SMALL-SIZED parabolic-trough solar collectors: Development of a test loop and evaluation of testing conditions. *Energy* **2018**, *152*, 401–415. [[CrossRef](#)]
43. Nain, S.; Ahlawat, V.; Kajal, S.; Anuradha, P.; Sharma, A.; Singh, T. Performance analysis of different U-shaped heat exchangers in parabolic trough sun ray collector for air heating applications. *Case Stud. Therm. Eng.* **2021**, *25*, 100949. [[CrossRef](#)]

Disclaimer/Publisher's Note: The statements, opinions and data contained in all publications are solely those of the individual author(s) and contributor(s) and not of MDPI and/or the editor(s). MDPI and/or the editor(s) disclaim responsibility for any injury to people or property resulting from any ideas, methods, instructions or products referred to in the content.